Vietnam Journal of Science and Technology ***62*** *(3) (2024)*

doi:10.15625/2525-2518/18503

Hemodynamics in Coronary Arteries: using Open-Source Software-Simvascular to Investigate the Hemodynamics in Coronary Arteries of the Patient-Specific Modeling

Nguyen Thi Dung, Do Thi Cam Nhung, Pham Thi Hue, Pham Van Sang*

Hanoi University of Science and Technology, No. 1 Dai Co Viet, Hai Ba Trung, Ha Noi, Viet Nam

*Email: *sang.phamvan@hust.edu.vn*

Received: 11 July 2023; Accepted for publication: 25 April 2024

Abstract. Patient-specific cardiovascular simulation is emerging as a potent tool for basic, translational, and clinical research and has established itself as a paradigm in the field of cardiovascular science. The SimVascular software package, considered a state-of-the-art open-source package, offers a comprehensive pipeline from medical imaging data segmentation to patient-specific blood flow simulation and analysis. In this study, we employ SimVascular to explore a model of coronary arteries in a young and healthy 24-year-old woman. The outcomes of the entire simulation process encompass the assessment of flow and pressure waveforms at both the outlet of the aorta and the coronary arteries, which serve as indicators of blood flow qualities within these vessels. Given the pivotal role of wall shear stress in the development of arterial plaque, SimVascular employs the finite element method to solve the governing equations of incompressible viscous fluids. This approach effectively tackles the Navier-Stokes equations along the vessel wall using meticulously constructed mesh components. Additionally, this paper delves into the issue of cardiovascular blood vessel dynamics via an analysis of wall shear stress data).

Keywords: Hemodynamics, Coronary arteries, Simvascular, Navier-Stokes equation, CFD.

Classification numbers: 5.4.4.

1. INTRODUCTION

Cardiovascular disease (CVD) is an umbrella term that includes several illnesses affecting the heart. Cardiovascular disease is the major cause of death worldwide. In 2019, 17.9 million people died from CDVs, accounting for 32 % of global mortality (World Health Organization, 2021) [1]. Blood vessel problems are one of the common heart diseases. Cardiovascular is a complicated system that involves non-Newtonian hemodynamics, electrophysiology, and biomechanics [2]. Besides, the heart's features (shape, structure, stiffness, electrical conductivity) affect its pumping ability. In addition, the heart is in constant motion, so extracting information

about the physiological processes is very difficult [3]. To specify hemodynamics conditions and evaluate mechanisms, simulation-based methods can solve this problem by simulating the realistic aspects of cardiovascular physiology. CFD (Computational Fluid Dynamic) is a branch of fluid mechanics and a specialist discipline of mathematics. CFD models are now employed in clinical settings to diagnose coronary and peripheral vascular diseases [4].

IBM (Image-based modeling) is a dominant tool in science and clinical research. IBM's practical example is HeartFlow Inc. Their application is in the diagnosis of coronary disease, which is characterized by a reduction in blood flow to the heart caused by cholesterol plaque accumulation. HeartFlow simulates the blood flow via a patient's arteries to determine various pressures [3]. A geometric model of a vascular region is created using 3D angiography data obtained from CT (computed tomography) or MRI (magnetic resonance imaging). A vascular geometry model is created using an image processing tool, which is then imported into a CFD package to generate a volumetric mesh and numerically simulate blood flow. There are a lot of CFD packages right now, but they are not suitable for simulating the specific physiological model and complicated boundary conditions of the cardiovascular system [5]. SimVascular was designed and developed at the lab of Charles Taylor in Standford to resolve the difficulty.

The most frequent type of heart disease is coronary artery disease (CAD) [6]. Ischemia is caused by plaque formation in the walls of the arteries that feed blood to the heart. Thus, understanding blood flow may determine the condition of the coronary from which to formulate optimal treatment plans for patients [7]. The blood flow in the coronary has the main characteristic of flow and pressure being out of phase, influenced by the contraction and relaxation of the heart. The highest blood flow in the coronary arteries happens during diastole. During systole the cardiac contracts, the coronary heart vessels constrict, and vascular resistance increases. During diastole, the heart muscle relaxes, the vascular resistance decreases, the blood flows speedily through the capillaries and coronary flow reaches maximum. Mantero *et al*. [8] created a lumped parameter model of coronary vascular beds coupled to each coronary outflow surface in 1992. SimVascular has specialized boundary conditions based on this model to mimic this characteristic. It is required to have a model of the heart and a model of the arterial system with consideration of how the two models interact in order to realistically model coronary artery flow and pressure. Zero-dimensional computation is used to solve this problem since coronary flow and pressure modeling is complex. Analogous electrical circuits are used to analyze vascular networks in a zero-dimensional (or lumped-parameter) formulation. When compared with the cost of a complete three-dimensional model, these simplified representations are computationally cheap [9,11].

2. MODEL GEOMETRY

2.1. The process of creating the solid mode

An MRI image file with DICOM format downloaded from the Wayback Machine - a digital archive of the World Wide Web founded by the Internet Archive is loaded to Simvascular. Standard Medical Imaging Interaction Toolkit (MITK) tools have been incorporated to Simvascular, including a display window with three orthographic 2D views and one 3D view in a flexible layout as shown in Figure 1(a).

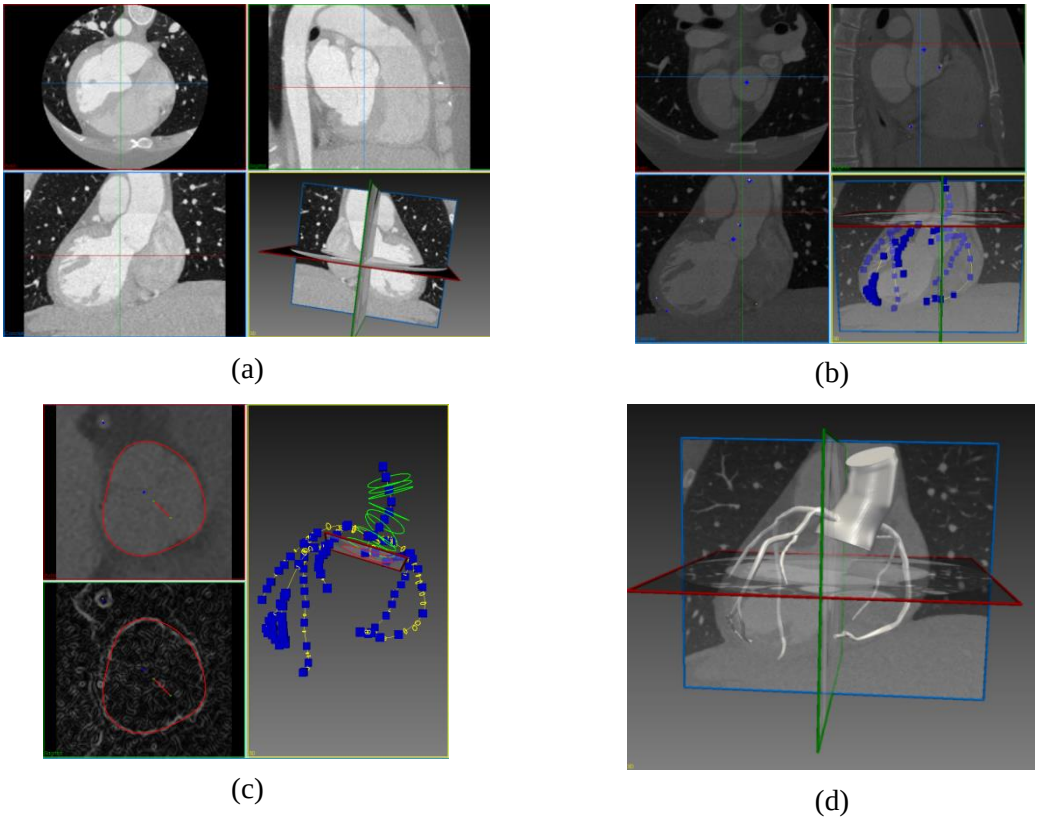

Figure 1. (a) An MRI image file with DICOM format of a healthy 24-year-old person loaded to Simvascular, (b) The paths of the aorta and coronaries are represented by a set of points, which are the approximate center of a vessel's lumen, (c) The segmentation of the aorta and coronary is created, (d) The created solid model represents a volume in space by a set of faces with well-defined boundaries connected to form a closed surface.

Then, a group of dots representing the aorta, right and left coronary artery, circumflex, and left anterior descending artery is constructed. Crosshairs are placed in the three 2D views to select the approximate center of a vessel lumen, and path points are then added interactively (Figure 1(b)). The next step is to produce segmentations, which entail extracting vessel lumen boundaries from imaging data using several image processing techniques. The development of solid models is based on these boundaries, which are represented by closed curves. A sequence of 2D picture slices is extracted from the image volume using paths made by Paths Tools. Each slice is then segmented in order to derive a lumen boundary. Segmentation points and intensity values are dynamically chosen from a 2D image as shown in Figure 1(c). Finally, a solid model depicts a volume in space by coupling a collection of faces with clearly defined boundaries to create a closed surface. Geometrically, the solid model's boundary faces are specified as polygonal or NURBS surfaces. A volume of vascular anatomy is geometrically represented using a solid model. By combining vessel surfaces that have been fitted to collections of 2D segmentations, it is constructed. The geometric information needed to create a finite element volumetric mesh is present in a solid model. The most popular solid modeler is PolyData - Faces, which represents solid models as surfaces made up of triangles (Figure 1(d)).

2.2. Creating the finite element mesh

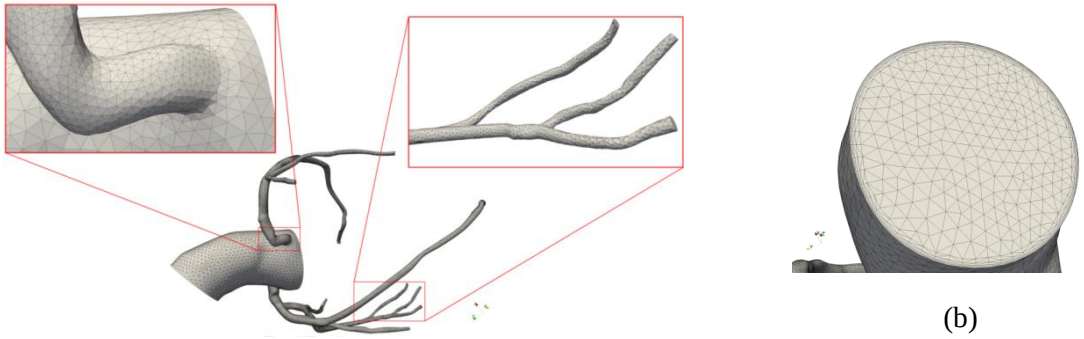

(a) (b)

Figure 2. a) Tetrahedral finite elements mesh. (b) The cells near the wall of the vessel are refined to resolve the nonlinearity of the variables in the Navier-Stokes equation for a Newtonian fluid

After having a solid model, we generate a mesh to simulate. A continuous volume enclosed by a solid model of vascular anatomy is divided into discrete tetrahedral elements using a mesh generation software. This finite element mesh is used by computational fluid dynamics programs to simulate blood flow in a vascular network.

3. MATHEMATICAL MODEL

3.1. Governing equation

It is possible to simulate the blood flow in the major vessels of the cardiovascular system using the flow of a Newtonian fluid. The incompressible Navier-Stokes equations are used to simulate blood flow, while the elastodynamics equations are used to model the motion of the vessel wall. The couple momentum method for fluid-solid interaction problem suggested and developed by Charles A. Taylor *et al*. for reducing the computational expensiveness of ALE (Arbitrarily Lagrangian - Eulerian) method [18] is used in our work. This means that we use a fixed fluid mesh assuming negligible displacements of the vessel wall. To solve the problem of vascular wall dynamics and blood flow in the solid and fluid domains, respectively, initial and boundary conditions, as well as fluid-solid interface conditions, must be satisfied in these equations. For a fluid domain Ω with its boundary Γ and a solid domain Ω^s with its boundary Ω_g^s the following equations are solved for velocities $\vec{v}$, pressure p, and wall displacement $\vec{u}$.

Given$\vec{f}: \Omega \times (0,T) \to \mathbb{R}^3, \vec{f}^s: \Omega^s \times (0,T) \to \mathbb{R}^3, \vec{g}: \Gamma_g \times (0,T) \to \mathbb{R}^3$, $\vec{g}^s: \Gamma_g^s \times (0,T) \to \mathbb{R}^3$, $\vec{v}_0: \Omega \to \mathbb{R}^3, \vec{u}_0: \Omega^s \to \mathbb{R}^3$, and $\vec{u}_{0,t}: \Omega^s \to \mathbb{R}^3$, find $\vec{v}(\vec{x},t)$, $p(\vec{x},t)$, and $\vec{u}(\vec{x}^s,t)$ for $\forall \vec{x} \in \Omega, \forall \vec{x}^s \in \Omega^s$ and $\forall t \in (0,T)$ such that the following conditions are satisfied:

$$\rho \vec{v}_{,t} + \rho \vec{v} \cdot \nabla \vec{v} = -\nabla p + div(\tilde{\tau}) + \vec{f}$$

for

$$(\vec{x},t) \in \Omega \times (0,T)$$
$$div(\vec{v}) = 0 \text{for} (\vec{x},t) \in \Omega \times (0,T)$$
$$\rho^s \vec{u}_{,tt} = \nabla \cdot \tilde{\sigma}^s + \vec{f}^s \text{for} (\vec{x}^s,t) \in \Omega^s \times (0,T) \quad (1)$$

where

$$\tilde{\tau} = \mu(\nabla \vec{v} + (\nabla \vec{v})^T)$$

and

$$\tilde{\sigma}^s = \tilde{C}:\frac{1}{2}(\nabla\vec{v} + (\nabla\vec{v})^T)$$

with the Dirichlet boundary condition,

$$\vec{v}(\vec{x},t) = \vec{g}(\vec{x},t)\text{for}(\vec{x},t) \in \Gamma_g \times (0,T)$$
$$\vec{u}(\vec{x}^s,t) = \vec{g}^s(\vec{x}^s,t)\text{for}(\vec{x}^s,t) \in \Gamma_g^s \times (0,T) \quad (2)$$

The Neumann boundary conditions,

$$\vec{t}_{\vec{n}} = [-p\,\tilde{I} + \tilde{\tau}]\vec{n} = \vec{h}(\vec{v},p,\vec{x},t)\text{for}\vec{x} \in \Gamma_h \quad (3)$$

The initial condition,

$$\vec{v}(\vec{x},0) = \vec{v}_0(\vec{x})\text{for}\vec{x} \in \Omega$$
$$\vec{u}(\vec{x}^s,0) = \vec{u}_0(\vec{x}^s)\text{for}\vec{x}^s \in \Omega^s$$
$$\vec{u}_{,t}(\vec{x}^s,0) = \vec{u}_{0,t}(\vec{x}^s)\text{for}\vec{x}^s \in \Omega^s \quad (4)$$

where the boundary $\boldsymbol{\Gamma}$ of the fluid domain is divided into a Dirichlet boundary portion $\boldsymbol{\Gamma_g}$ and a Neumann boundary portion $\boldsymbol{\Gamma_h}$. Similarly, the boundary $\boldsymbol{\Gamma^s}$ of the solid domain is divided into Dirichlet boundary portion and a Neumann boundary condition portion. They satify $\overline{(\boldsymbol{\Gamma_h} \cup \boldsymbol{\Gamma_g})} = \boldsymbol{\Gamma}$, $\overline{(\boldsymbol{\Gamma^s_h} \cup \boldsymbol{\Gamma^s_g})} = \boldsymbol{\Gamma^s}$, $\boldsymbol{\Gamma_h} \cap \boldsymbol{\Gamma_g} = \emptyset$ and $\boldsymbol{\Gamma^s_h} \cap \boldsymbol{\Gamma^s_g} = \emptyset$. The external body force on the fluid domain is represented by $\vec{\mathbf{f}}$. Similarly, the $\vec{\mathbf{f}}^{\mathbf{s}}$ is the external body force on the solid domain. $\widetilde{\mathbf{C}}$ is a fourth-order tensor of material constants, and $\tilde{\boldsymbol{\sigma}}^{\mathbf{s}}$ is the vessel wall stress tensor. $\boldsymbol{\rho} = \mathbf{1.06\ g/cm^3}$ which is the density of the blood, $\boldsymbol{\mu} = \mathbf{0.04\ dynes/cm^2}$ – which is - the dynamic viscosity of the fluid, and $\boldsymbol{\rho^s} = \mathbf{1.0\ g/cm^3}$ is - the density of the vessel walls are assumed to be constant [17].

The SimVascular solver solves the incompressible viscous fluid equations using the finite element algorithm. SimVascular's flow solver evolved from the academic finite element code PHASTA (Parallel, Hierarchical, Adaptive, Stabilized, Transient Analysis) for solving the Navier-Stokes equations in any domain using the streamline-upwind/Petrov Galerkin (SUPG) and pressure-stabilizing/Petrov Galerkin (PSPG) methods. The SUPG/PSPG formulation is defined on the trial solution and weight function spaces in finite dimensions.

3.2. The boundary condition of the model

In an earlier study, Vignon-Clementel *et al*. [10] developed boundary conditions for three-dimensional models of blood flow that could simulate each subject's physiological parameters. In this study, we use a zero dimension model to simulate hemodynamics in the coronary artery system. Unlike 3D and 1D models, 0D models are time-dependent. Our lowest-fidelity model is a lumped parameter network description of blood flow. This circuit layout was created using an analogy to hydrodynamics, where the flow rate is represented by electrical current, and pressure changes are represented by voltage, and each circuit component is related to an algebraic or differential equation, i.e. resistor $\Delta P = RQ$, capacitor $Q = C\,dP/dt$, and inductor $\Delta P = L\,dQ/dt$.These equations are combined to form an ODE system that can be efficiently solved, for example, with a 4th-order Runge-Kutta scheme. Resistors are utilized to simulate viscous dissipation on vessel walls, capacitors to simulate vascular tissue compliance, and inductors to simulate blood inertia. The model parameters for these circuit parts are determined using the Poiseuille flow assumption [12], i.e.$R = \frac{8\mu l}{\pi r^4}$, $C = \frac{3l\pi r^3}{2Eh}$, $L = \frac{l\rho}{\pi r^3}$ where μ is the dynamic viscosity of blood, L the vessel length, R the vessel radius, E the elastic modulus, h the wall thickness, and

ρ the density of blood. These models have been widely used to simulate the heart and circulatory system, producing remarkably realistic flow and pressure waveforms and enabling the assessment of physiologic changes in response to therapies [12,13]

The assignment of the boundary condition of the simulation process is shown in Figure 3, where the inlet boundary condition for the aorta is directly prescribed with the flow rate condition at the aorta. This condition basically assigns the time history of the aorta flow waveform, which is measured by PC-MRI at the Asc A_0 plane highlighted in the aortic geometry. The flow waveform curve, which is marked with the red ellipse in Figure 3, is used in this work. It usually goes with a mean flow rate (Q_m) of around 100 mL/sec.The outlet of the aorta boundary condition is attached like three-element (RCR) Windkessel models to incorporate the resistance and also the capacitance effect of downstream blood vessels with $R_d = 1421.86$, $R_p = 140.63$, and $C = 0.001$ cm^2/dyne which were determined to match the subject-specific pulse pressure and cardiac output [16].

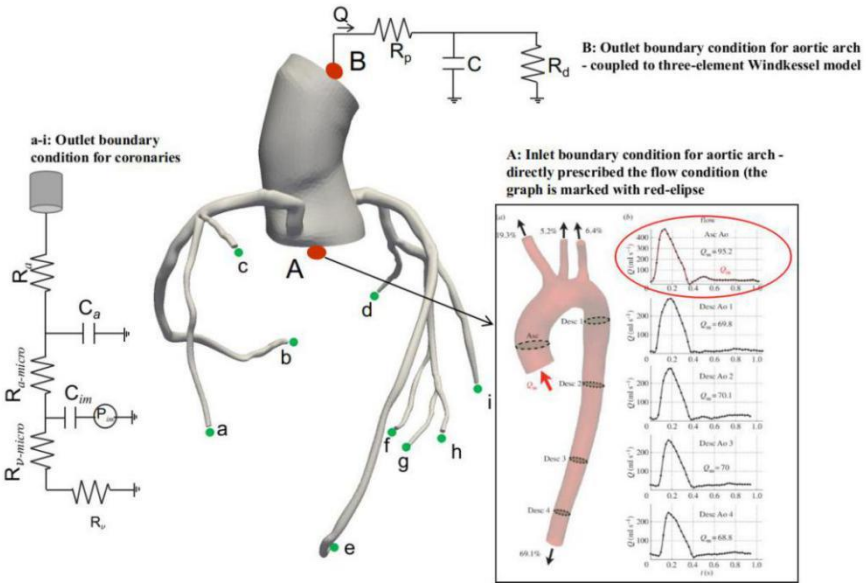

Figure 3. Problem specification of the aortic arch inlet, outlet, and coronary outlets for blood flow simulations in an aorta arch model with coronary outlets. Note that all of the three-dimensional computational model's outlets flow back into the lumped model.

At the outlet of the coronary arteries, a specialized boundary condition is needed due to their unique physiology. Unlike other arteries, the coronary artery experiences low pressure during systole because the contracting heart muscle impedes fluid flow [14]. In contrast, during diastole, as the heart muscle relaxes, the flow in the coronary arteries peaks. This is different from the aorta, where pressure rises in systole and falls in diastole. The distinct coronary waveform is due to the heart muscle's contraction and relaxation phases affecting blood flow. In order to model the boundary condition at the outlet of the coronary artery, which is the coronary artery bed, the model of electric-hydraulic analogy needs multiple circuit elements, including

coronary arterial resistance R_a, coronary arterial compliance C_a , coronary arterial microcirculation resistance $R_{a-micro}$, myocardial compliance C_{im} , coronary venous microcirculation resistance $R_{v-micro}$, coronary venous resistance R_μ , and intramyocardial pressure $P_{im}(t)$. To determine the circuit element values, the physiological rule of 4.0 % is applied, which means that the mean coronary flow is 4.0 % of the cardiac output and Murray's law governs the hemodynamics inside the coronary arteries [15,16].

4. RESULTS AND DISCUSSIONS

In the simulation process, we examined coronary flow and pressure in light conditions. The refined mesh, which has the refining of the cells near the wall of the vessel, is performed to resolve the nonlinearity of the variables in the Navier-Stokes equation for Newtonian fluids. The information of the finite element mesh contains number of nodes: 58382, number of elements: 301387, number of edges: 58647, and number of faces: 39098. All simulations were run on a Dell M4800 workstation with an Intel i7, 2.4 GHz, 8 CPU, and 8 GB of RAM. The solutions were run until the relative pressure fields at the intake and outflow did not differ by more than 1.0 % from those in the previous cardiac cycle's solutions at the same phase.

4.1. Hemodynamics quantities of the blood flow in the coronary arteries

The pressure distribution in the aorta and the coronary artery is shown in Figure 4, which displays conformance to the physical characteristics in the transport of blood in the aorta and coronary arteries. Specifically, since the model is a part of the aorta located right next to the outlet of the left ventricle, the pressure in the aorta part is high, shown in red with a color scale of 95 mmHg for the entire aorta part. At coronary artery branches near the aorta the pressure is almost unchanged. Meanwhile, the pressure drops significantly near the end of coronary artery branches. The change in pressure occurs most clearly when the blood flows away from the aorta or in other words it occurs near the end of the coronary artery branches. However, because the length of these branches is not too large and their cross-section is much smaller than that of the aorta, the pressure does not change too much. The difference between the maximum value (95 mmHg) and minimum value (82 mm Hg) of pressure is only 13.7 %.

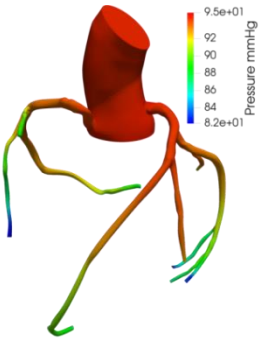

Figure 4. The pressure distribution in the aorta and the coronary artery.

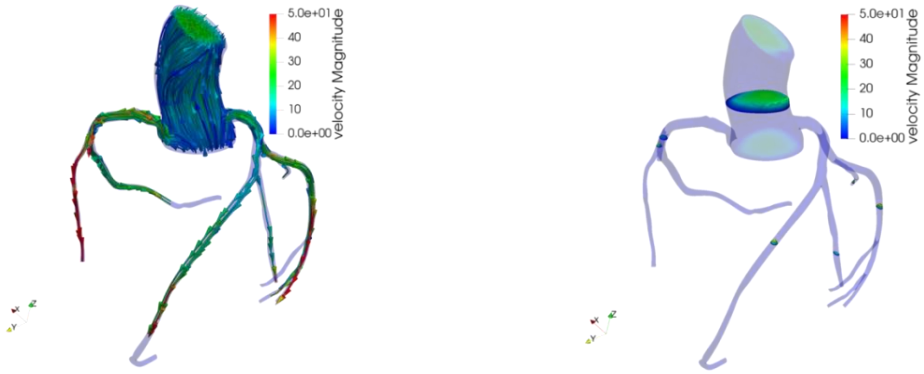

(a) (b)

Figure 5. The flow velocity field in the aorta and the coronary arteries. (a) Blood flow is displayed with streamlines with the arrow used to indicate the direction of flow velocity. (b) The flow velocity magnitude is warped by scalar in some cross-section of the model.

The physiological properties of intravascular blood transport, where the velocity of flow near the vessel wall is close to zero, are mimicked by applying a no-slip condition to the wall boundary. From Figure 5(a), we can see the streamlines at the wall boundary with the darkest green color, showing that the no-slip condition was observed during the simulation process. The magnitude of the velocity is greatest at the center of the blood vessel, as shown by the gradient of color. As can be seen, the magnitude of the flow velocity at the end of the coronary arteries is higher compared to that in the aorta. This happens due to a decrease in the cross-section area of the vessel.

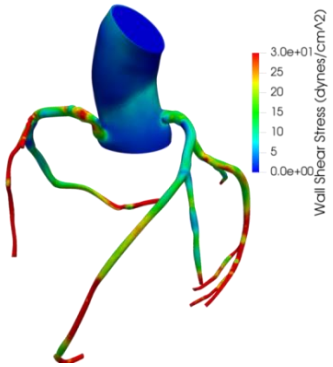

Figure 6. The aortic and coronary artery wall shear stress.

The frictional force on the vessel wall, known as wall shear stress (WWS), plays an important role in the natural history of atherosclerotic plaque development [18]. So the result of wall shear stress is the important result of the hemodynamics simulation. From the distribution of wall shear stress of a vessel, we can make judgments of vulnerable locations if there is a sudden increase in pressure or external force. The value of wall shear stress is high at the end of the coronary artery branches and the position where there is a sudden change in shape. These locations are easy to cause obstruction of blood flow. From Figure 6, we can see the simulation results accurately reflect the phenomenon occurring in blood circulation in blood vessels. At the

position where the obstruction can easily take place, the position has a small cross section or an abrupt change in vascular shape.

4.1. Hemodynamics quantities of the blood flow in the coronary arteries

In Figure 7(a), the pressure at the inlet aorta is between ~120 mmHg and ~80 mmHg, it is appropriate for normal blood pressure level. Peak-to-peak amplitude would be too low if the RCR compliance had been too high, i.e., the systolic pressure would be ~110 mmHg and the diastolic pressure would be ~90 mmHg. If the aortic compliance were too low, the opposite would be true. For matching the specific patient's data the RCR compliance is tuned appropriately. As we can see in Figure10(b), the aortic outlet boundary has the shape of graph flow rate similar to that of the aortic inlet boundary. The result is conformable according to the 4 % rule as described in the previous section. The mean outlet pressure seems to be between ~120 mmHg and~80 mmHg. However, the slope of pressure in the range from 6th to 11th time-step is slighter compared to that in the aortic inlet boundary.

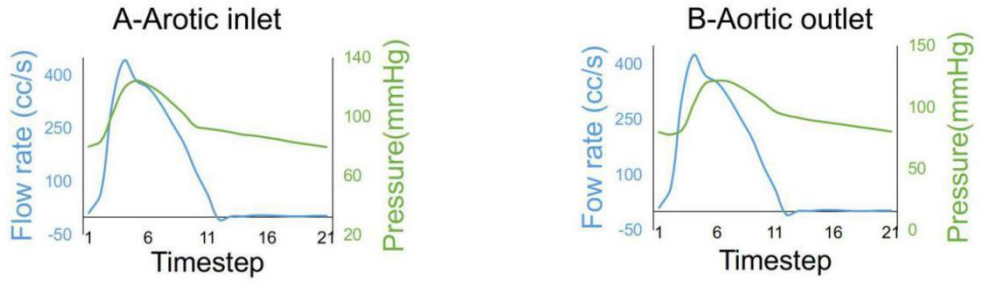

(a) (b)

Figure 7. Pressure is displayed by the green line with the green secondary vertical axis and flow rate is displayed by the blue line with the blue primary vertical axis. (a) Pressure and flow rate at the aortic inlet boundary. (b) Pressure and flow rate at the aortic outlet boundary.

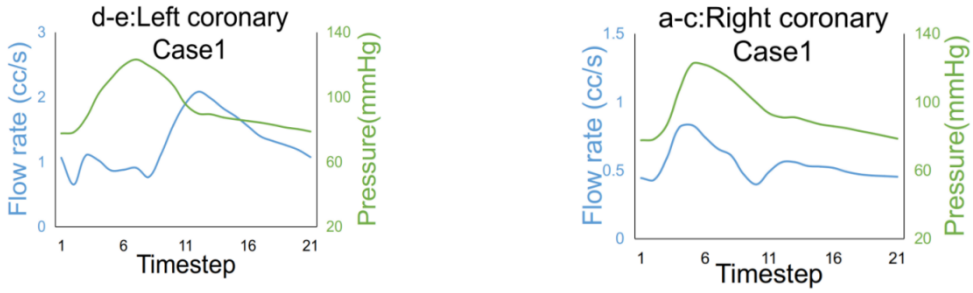

(a) (b)

Figure 8. Pressure is displayed by the green line with the green secondary vertical axis and flow rate is displayed by the blue line with the blue primary vertical axis. (a) Pressure and flow rate at the left coronary arteries outlet boundary. (b) Pressure and flow rate at the right coronary arteries outlet boundary.

Figure 8 shows the left and right coronary waveforms during the systole and diastole. In systole, the left and coronary waveform has a small slope and a mean flow rate of 0.85 cc/s. In contrast, the right coronary flow rate waveform is relatively small compared with that value and has a larger slope and a peak flow rate roughly equal to the mean flow rate of the left coronary.

In diastole, meanwhile, the left coronary waveform has a larger slope and a flow peak of 2 cc/s, and the right coronary waveform has a gentle slope and a relatively small mean value. Because during systole, blood is pumped out of the heart, the left side of the heart is where most of the work is done, and the right side of the heart is the place that doesn't do much. Therefore, the left coronary waveform has a smaller flow rate during systole than the right coronary waveform. During diastole, blood flows back into the heart. The left and right coronary waveforms both receive blood, so they have relatively equal peak flows. So the coronary waveforms exhibit the expected behavior

5. CONCLUSIONS

Using Simvascular, a cutting-edge cardiovascular modeling software, researchers studied flow, pressure waveform of blood flow, and blood vessel wall shear stress. To more accurately describe flow and pressure waveforms, we took into account fluid-structure interaction. Using anatomic information gleaned through medical imaging methods, the lumped parameter coronary vascular model, and the inflow boundary condition connecting the lumped parameter heart model and the open loop system, we can accurately estimate coronary flow and pressure. We can also investigate the relationship between changes in coronary flow and pressure and changes in cardiac and arterial characteristics. These methods can also be used to investigate potential vascular therapies for cardiovascular disease.

Acknowledgements. This research was funded by the Ministry of Education and Training under Project No. T2021-PC-040. Dung T. Nguyen was funded by the Master, PhD Scholarship Programme of the Vingroup Innovation Foundation (VINIF), code VINIF.2022.ThS.014..

CRediT authorship contribution statement. Nguyen Thi Dung and Pham Thi Hue: Methodology, Investigation, Funding acquisition. Nguyen Thi Dung and Do Thi Cam Nhung: Formal analysis, Proof reading. Pham Van Sang Supervision, Proof reading.

Declaration of competing interest. The authors declare that they have no known competing financial interests or personal relationships that could have appeared to influence the work reported in this paper.

REFERENCES

1. World Health Organization Model List of Essential Medicines – 22nd List, 2021. Geneva: World Health Organization; 2021 (WHO/MHP/HPS/EML/2021.02). Licence: CC BY-NC-SA 3.0 IGO.
2. Lee, B.-K. (2011). Computational Fluid Dynamics in Cardiovascular Disease. Korean Circulation Journal, 41(8), 423. doi:10.4070/kcj.2011.41.8.423.
3. Nguyen, T. D., Kadri, O. E., & Voronov, R. S. (2020). An Introductory Overview of Image-Based Computational Modelling in Personalized Cardiovascular Medicine. Frontiers in Bioengineering and Biotechnology, 8. doi:10.3389/fbioe.2020.529365.
4. Morris, P. D., Narracott, A., von Tengg-Kobligk, H., Silva Soto, D. A., Hsiao, S., Lungu, A., … Gunn, J. P. (2015). Computational fluid dynamics modelling in cardiovascular medicine. Heart, 102(1), 18–28. doi:10.1136/heartjnl-2015-308044.
5. Updegrove, A., Wilson, N. M., Merkow, J., Lan, H., Marsden, A. L., & Shadden, S. C. (2016). SimVascular: An Open-Source Pipeline for Cardiovascular Simulation. Annals of Biomedical Engineering, 45(3), 525–541. doi:10.1007/s10439-016-1762-8.

6. Dheeraj Mehta et al. “Towards the prevention of vein graft failure”. In: International journal of cardiology 62 (1997), S55–S63. DOI: 10.1016/s0167-5273(97) 00214-3.
7. Mahdi Esmaily-Moghadam et al. “The assisted bidirectional Glenn: a novel surgical approach for first-stage single-ventricle heart palliation”. In: The Journal of thoracic and cardiovascular surgery 149.3 (2015), pp. 699–705. DOI: 10.1016/j. jtcvs.2014.10.035.
8. Mantero, S., Pietrabissa, R., & Fumero, R. (1992). The coronary bed and its role in the cardiovascular system: a review and an introductory single-branch model. Journal of Biomedical Engineering, 14(2), 109–116. doi:10.1016/0141-5425(92)90015-d.
9. Yogeswaran, Swetha, and Fei Liu. Vascular Flow Simulations Using SimVascular and OpenFOAM. Cold Spring Harbor Laboratory, Sept. 2021. Crossref, doi:10.1101/2021.09.11.21263191.
10. Irene E Vignon-Clementel et al. “Outflow boundary conditions for three-dimensional finite element modeling of blood flow and pressure in arteries”. In: Computer methods in applied mechanics and engineering 195.29-32 (2006), pp. 3776–3796. DOI: 10.1016/j.cma.2005.04.014.
11. Wan, J., Steele, B., Spicer, S. A., Strohband, S., Feijo´o, G. R., Hughes, T. J. R., & Taylor, C. A. (2002). A One-dimensional Finite Element Method for Simulation-based Medical Planning for Cardiovascular Disease. Computer Methods in Biomechanics and Biomedical Engineering, 5(3), 195–206. doi:10.1080/10255840290010670
12. Kung, E., Baretta, A., Baker, C., Arbia, G., Biglino, G., Corsini, C., … Migliavacca, F. (2013). Predictive modeling of the virtual Hemi-Fontan operation for second stage single ventricle palliation: Two patient-specific cases. Journal of Biomechanics, 46(2), 423–429. doi:10.1016/j.jbiomech.2012.10.023
13. Kim, H. J., Vignon-Clementel, I. E., Figueroa, C. A., LaDisa, J. F., Jansen, K. E., Feinstein, J. A., & Taylor, C. A. (2009). On Coupling a Lumped Parameter Heart Model and a Three-Dimensional Finite Element Aorta Model. Annals of Biomedical Engineering, 37(11), 2153–2169. doi:10.1007/s10439-009-9760-8
14. Roberto Burattini et al. “Identification of canine coronary resistance and intramyocardial compliance on the basis of the waterfall model”. In: Annals of biomedical engineering 13.5 (1985), pp. 385–404. DOI: 10.1007/BF02407768
15. Barry, W. H. (2004). Heart Physiology From Cell to Circulation, 4th ed. Circulation, 110(12), e313–e313. doi:10.1161/01.cir.0000143724.99618.62
16. Burattini, R., Sipkema, P., van Huis, G. A., & Westerhof, N. (1985). Identification of canine coronary resistance and intramyocardial compliance on the basis of the waterfall model. Annals of Biomedical Engineering, 13(5), 385–404. doi:10.1007/bf02407768
17. Kim, J. Y., Yoon, J., Cho, M., Lee, B. K., Karimi, A., & Shin, S. (2013). Blood characteristics effect on pulse wave velocity. Clinical Hemorheology and Microcirculation, 55(1), 193–203. https://doi.org/10.3233/ch-131702.
18. Figueroa, C. A., Vignon-Clementel, I. E., Jansen, K. E., Hughes, T. J. R., & Taylor, C. A. (2006). A coupled momentum method for modeling blood flow in three-dimensional deformable arteries. Computer Methods in Applied Mechanics and Engineering, 195(41-43), 5685–5706. doi:10.1016/j.cma.2005.11.011